Sensors and Actuators: A. Physical 337 (2022) 113191

Contents lists available at ScienceDirect

Sensors and Actuators: A. Physical

journal homepage: www.elsevier.com/locate/sna

Electromagnetic radiation detection using cantilever-based photoacoustic effect: A method for realizing power detectors with broad spectral sensitivity and large dynamic range

Sucheta Sharma[a,*], Toni Laurila[a], Jussi Rossi[b], Juho Uotila[c], Markku Vainio[b,d], Farshid Manoocheri[a], Erkki Ikonen[a,e]

[a] Metrology Research Institute, Aalto University, Maarintie 8, FI-02150 Espoo, Finland
[b] Photonics Laboratory, Tampere University, Korkeakoulunkatu 7 Kampusareena, 33720 Tampere, Finland
[c] Patria Aviation Oy, Hatanpään valtatie 30, 33100 Tampere, Finland
[d] Department of Chemistry, University of Helsinki, PB 55 (A. I. Virtasen aukio 1), 00014 Helsinki, Finland
[e] VTT MIKES, Tekniikantie 1, 02150 Espoo, Finland

ARTICLE INFO

Article history:
Received 1 April 2021
Received in revised form 17 September 2021
Accepted 19 October 2021
Available online 23 October 2021

Keywords:
Photoacoustic
Soot
Detectors
Optical metrology
Radiation detection
Photoacoustic numerical model
Cantilever pressure sensor

ABSTRACT

A sensitive photoacoustic detection approach employing a silicon cantilever is investigated for power measurement of electromagnetic radiation. The technique which is actuated by pressure waves generated through radiation-induced heat depicts high sensitivity for a considerably large spectral range from 325 nm to 1523 nm. The implemented method shows linear response in the measurement of radiation power from 15 nW to 6 mW demonstrating a dynamic range of almost six orders of magnitude. A numerical model has been developed to analyze and optimize the measurement sensitivity. The model allows studying different dimensions of the cantilever which is one of the key components of the radiation detection process. The numerical results are in good agreement with experimental results. The electromagnetic power detection technique shows future potential for industrial applications and scientific studies.

1. Introduction

Photoacoustic (PA) effect is based on detecting pressure waves in a fluid medium, produced by the absorption of short-pulsed or modulated electromagnetic radiation [1,2]. Two key components, light absorbing medium and a pressure sensor [3–6], play major roles in such detection systems. Because of the constructional simplicity and detection sensitivity, the PA technique serves as a powerful tool for numerous applications in the field of high-resolution imaging, microscopy and in spectroscopic sensing of toxic, inflammable and explosive gases or particulate environmental pollutants which pose major risk on health, safety and security [7–14]. For applications in the field of traceable measurement of radiation power, important prerequisites include a suitable radiation absorber material that responds to optical excitation along with a sensitive pressure detection technique that commonly employs electrical or optical methods [15,16]. The underlying mechanism is based on the measurement of pressure waves activated by radiation-induced heat generation in the optical absorber.

One of the common pressure detection methods in PA uses capacitive microphones. However, technologies with capacitive membrane microphones suffer from limitations such as the non-linear response of the membrane in sensing the external pressure. Apart from that, for sensitivity improvement, there is a limitation below which the gap between the membrane and the backplane of the capacitive condenser cannot be reduced to avoid viscous effect of the gaseous medium [15]. The optical pressure sensing approach, on the other hand, is realised by monitoring the light beam deflected from elastic membranes or micro-mechanical silicon-cantilevers [16,17]. Cantilevers avoid some of the drawbacks of capacitive microphones, hence, they are used in applications requiring very high sensitivity. The periodical heat-induced volume expansion of the carrier fluid causes mechanical movement of the cantilever. A compact interferometer is used to detect such movement of the cantilever tip [16]. The amplitude of the generated PA signal is

* Corresponding author.
E-mail address: sucheta.sharma@aalto.fi (S. Sharma).

https://doi.org/10.1016/j.sna.2021.113191
0924-4247/

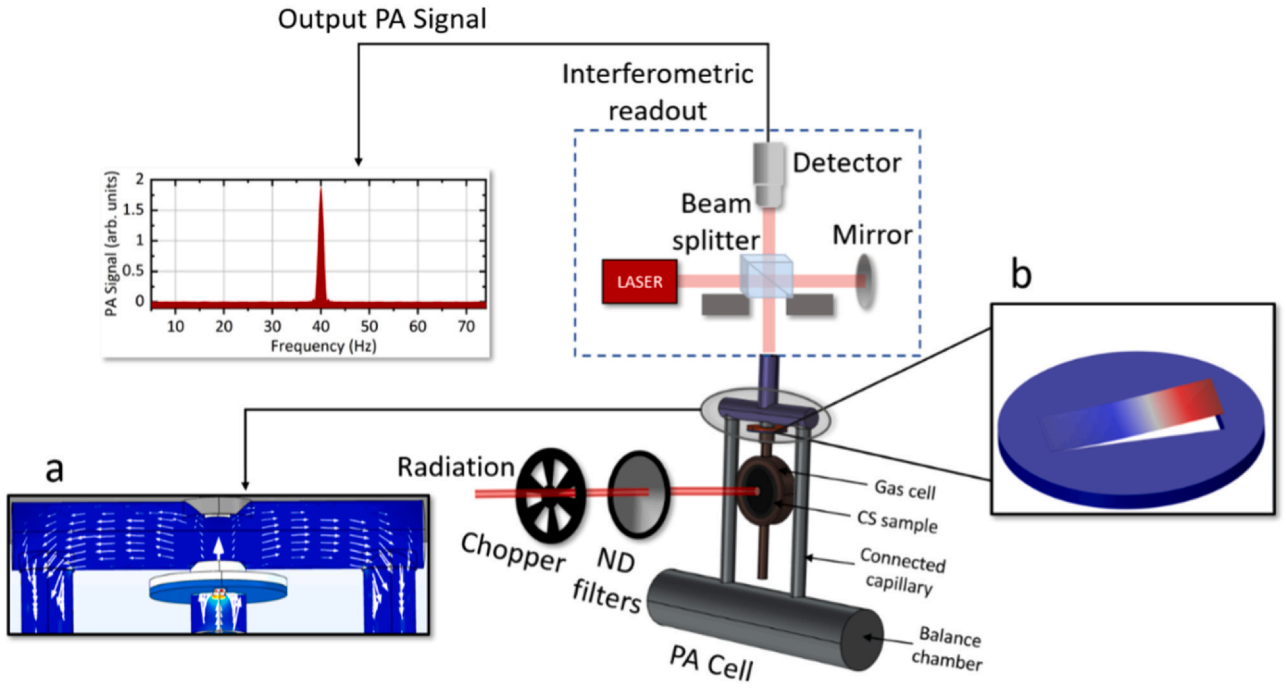

Fig. 1. Schematic representation of the PA radiation detection system. The system consists of three subsystems to convert input radiation to heat by using CS (candle soot) absorber target, to produce mechanical response with the cantilever and, finally, to generate the PA signal from interferometric readout. There are two main gas domains: primary gas cell which directly heats up when the connected CS absorbs radiation and the balance chamber along with two capillaries that reduces the acceleration noise in the system. a. Velocity diagram of gaseous medium within the PA cell. The arrows represent how the induced pressure interacts with the cantilever to generate mechanical response. b. Cantilever being displaced due to the generated pressure within the PA cell. The highest displacement zone is concentrated at the tip of the cantilever.

directly proportional to the power of incident radiation. The technique works at room temperature without any need for cryogenic cooling.

Many different power detection techniques exist, yet they all have limitations in terms of spectral coverage and dynamic range. Most available semiconductor power detectors have spectral responsivity, which depends on the operating wavelength [18]. Pyroelectric detectors are excellent in sensing electromagnetic radiation over a wide spectral range with the noise floor for power measurement near 1 μW [19,20]. Golay cell is a well-known detection technology which uses the PA principle. With proper window material, commercial Golay cells can cover a wide spectral range with the highest measurable power in the μW range [21].

In this work, the potential of a cantilever-based pressure sensor is studied in PA detection of radiation power. The proposed approach can be applied over the spectral range from Ultraviolet (UV) to near infrared (NIR). We have developed a numerical model to study the frequency response and signal strength of cantilevers of different dimensions to optimise the detection sensitivity. With the present method, the upper limit of detection can be made considerably high. To our knowledge, the analysis on optimising the detection sensitivity and improving the dynamic range of such systems for the applications of optical power detection has not been reported earlier. Benefits of the proposed PA power measurement method include good linearity and broad spectral range. Here we have characterised the method for the wavelengths between 325 nm and 1523 nm. Measurements have been carried out in the range 15 nW - 6 mW, demonstrating the dynamic range of almost six orders of magnitude.

2. Experimental setup and methods

The schematic diagram of the experimental arrangement is shown in Fig. 1. The PA radiation-detection method is a combination of energy conversion processes: optical to thermal energy, which is followed by thermal to mechanical energy conversion. The experimental procedure is governed by three constitutive mechanisms: (i) Excitation using electromagnetic radiation; (ii) Temperature and pressure induced mechanical response; (iii) Optical detection of the mechanical response and generation of the output PA signal. To actuate the mechanical response, the system requires absorbing materials which efficiently convert optical energy to thermal energy. Studies have been carried out suggesting several black absorbing carbon-based materials such as carbon nanotubes, carbon black powders, carbon nanofibers [22–25], to name a few.

Candle soot (CS) is also a good candidate because of its cost-effective manufacturing process and strong PA response [26]. In the experimental setup here the laser radiation first passes through a chopper, which produces intensity modulation of electromagnetic radiation that falls on the CS absorber. Here the frequency of the beam chopping was kept fixed at 40 Hz to achieve good signal-to-noise ratio. Fig. 2 shows the measured spatial response map of the CS absorber surface which was used in this study. The spatial uniformity was measured using a 442 nm laser source with a beam diameter of about 1.4 mm.

The output PA signal as shown in the diagram of Fig. 1 represents the response of the cantilever to the intensity variation of the radiation source at the 40 Hz chopping frequency. By using variable

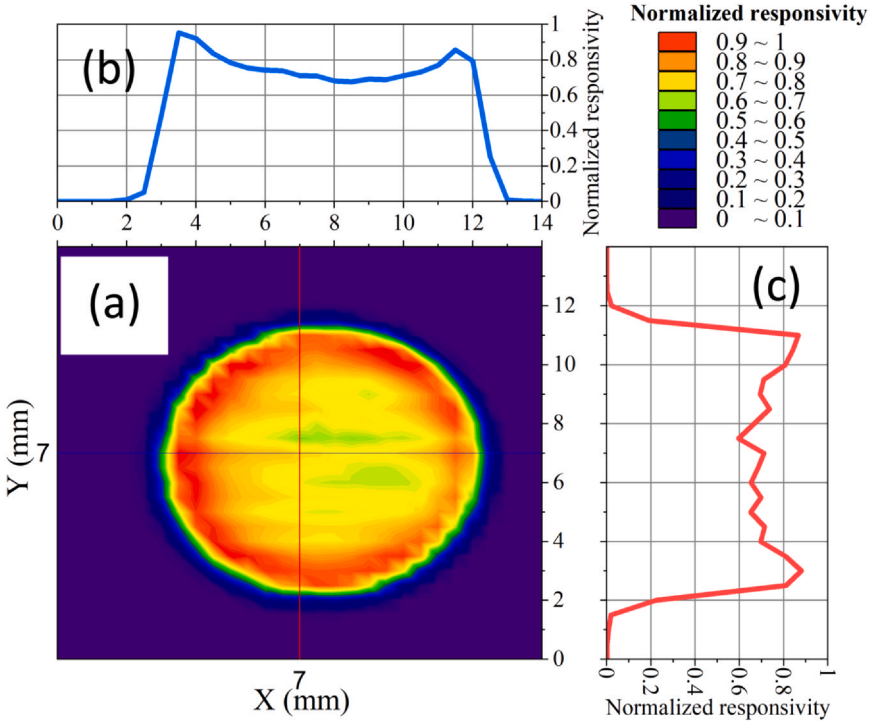

Fig. 2. Spatial scan of the CS surface performed using 442 nm laser (a) The color distribution indicates the variation of the PA signal strength. (b) Normalized responsivity for the scanned region X = 0 – 14 mm and Y = 7 mm (indicated by horizontal line on the color map in (a)). (c) Normalized responsivity for the scanned region X = 7 mm and Y= 0 – 14 mm (indicated by vertical line in (a)). (For interpretation of the references to colour in this figure, the reader is referred to the web version of this article.)

neutral density (ND) filters the power of the input radiation was attenuated to study the detector's response to varying power levels. The amplitude of PA signal for a given incident radiation can be expressed as: $S_{PA} = \sigma_{PA} P$ where σ_{PA} is the detection sensitivity and P is the power of incident radiation. The sensitivity σ_{PA} depends on the properties of the light absorber, the PA cell and the cantilever. Thus, the cantilever has a significant role in improving the PA system response. To improve σ_{PA} we have focused on the cantilever design by mainly analyzing the suitable dimensions. In addition to the deflection amplitude of the cantilever, the resonance frequency is also an important factor for achieving better overall system performance. In order to have system stability where small changes in modulation frequency do not induce large PA amplitude changes, the operating frequency is generally chosen lower than the resonance frequency of the system. Hence, a proper design of the cantilever is important to optimize both sensitivity and frequency response.

3. Numerical model

We have developed a numerical model of the experimental setup using COMSOL Multiphysics® v. 5.4.0.388. The PA cell with gas cell radius of 6.3 mm and height of 3.3 mm, contains the gaseous medium, e.g., air or helium (He), under a background pressure which is modified when the medium is exposed to periodic temperature variation.

For small perturbations around the steady background values, the dependent variables take the form

$$p = p_b + p' e^{j\omega t} \tag{1}$$

$$\boldsymbol{u} = \boldsymbol{u_b} + \boldsymbol{u}' e^{j\omega t} \tag{2}$$

$$T = T_b + T' e^{j\omega t} \tag{3}$$

$$\rho = \rho_b + \rho' e^{j\omega t}, \tag{4}$$

where p is the pressure, $\boldsymbol{u}$ is velocity field, T is temperature, ρ is fluid density and ω is angular frequency. The background pressure, velocity, temperature and fluid density are p_b, $\boldsymbol{u_b}$, T_b and ρ_b, respectively. It can be assumed that there is no contribution of background velocity, thus $\boldsymbol{u_b} = 0$. The values of T_b and p_b were chosen to be 293 K and 1013.25 hPa, respectively. The corresponding acoustic responses are represented by the primed variables. The governing equations are the momentum equation, continuity equation and energy equation. In the frequency domain, by omitting the primed notations, the equations are expressed as

$$j\omega\rho_b \boldsymbol{u} = \nabla\cdot[-p\boldsymbol{I} + \mu(\nabla\boldsymbol{u} + (\nabla\boldsymbol{u})^T) - ((2/3\mu) - \mu_B)(\nabla\cdot\boldsymbol{u})\boldsymbol{I}] \tag{5}$$

$$j\omega\rho + \nabla\cdot(\rho_b \boldsymbol{u}) = 0 \tag{6}$$

$$\rho_b C_p (j\omega T + \boldsymbol{u}\cdot\nabla T_b) - T_b \alpha_p (j\omega p + \boldsymbol{u}\cdot\nabla p_b) = \nabla\cdot(K\nabla T) + Q. \tag{7}$$

Parameters μ, μ_B, C_p, $\boldsymbol{I}$, Q and K are the dynamic viscosity, bulk viscosity, heat capacity at constant pressure, unit tensor, heat source and thermal conductivity, respectively [27]. In addition to the above equations, there is the linearized equation of state, $\rho = \rho_b(\beta_T p - \alpha_p T)$ where α_p is the coefficient of thermal expansion and β_T is the isothermal compressibility. In the case of air and He as the gaseous media, the expressions for α_p and β_T can be considered under the case of ideal gas approximation where the value of α_p is the inverse of T_b and β_T is the inverse of p_b.

Table 1 summarizes the input parameters of the numerical model. The remaining input parameters include the density ρ_{Si},

Table 1
Constituting material parameters of the numerical model.

Model parameters	Air	He
K (W/m K)	0.02565	0.14929
C_p (J/kg K)	1015.12	5196.49
ρ_b(kg/m^3)	1.2032	0.1663
μ (Pa s)	1.817×10^{-5}	1.973×10^{-5}
μ_B (Pa s)	1.81×10^{-5}	1.96×10^{-5}

Table 2
Comparison between experiment and simulation for calculating the resonance frequency (f_0) of the PA detection system with cantilever-I.

Material	$f_0\|_{Sim.}$ Hz	$f_0\|_{Expt.}$ Hz	Relative difference $\frac{(f_0\|_{Expt.} - f_0\|_{Sim.})}{f_0\|_{Sim.}} \times 100\,\%$
Air	690	700	+ 1.5%
He	920	830	- 9.8%

Table 3
Responses and resonance frequencies of cantilevers of different dimensions for gaseous medium air and He.

Cantilever	Dimensions	PA response (arb. units) at ~ 40 Hz		$f_0\|_{Sim.}$ (Hz)	
		Air	He	Air	He
Cantilever-I	6 mm × 0.7 mm × 5 µm	0.83	0.79	690	920
Cantilever-II	6 mm × 0.7 mm × 10 µm	0.72	0.68	710	970
Cantilever-III	4 mm × 0.7 mm × 10 µm	0.53	0.48	910	1140
Cantilever-IV	4 mm × 1 mm × 10 µm	0.45	0.41	910	1240

Young's modulus E and Poisson's ratio ν of the cantilever material silicon, which are 2329 kg/m^3, 170 × 10^9 Pa and 0.28, respectively. The thickness of the viscous boundary layer is given by $\delta_{visc} = \sqrt{2\mu/\omega\rho_b}$. The layer thicknesses for air and He at 40 Hz, 20° C and 1013.25 hPa are thus 0.348 mm and 0.972 mm, respectively. The value of Prandtl number (P_r), $P_r = \delta_{visc}{}^2/\delta_{therm}{}^2$ is 0.7 for air and 0.69 for He, where $\delta_{therm} = \sqrt{2K/\omega\rho_b C_p}$ is the thermal boundary layer thickness [28,29].

To validate the model, the frequency response of the system with a cantilever (cantilever-I) having dimensions 6 mm × 0.7 mm × 5 µm (length × width × thickness) was first compared with the experimental data. Table 2 and Fig. 3 show the comparison between the experimentally and numerically obtained data on the resonance frequency of the system. As shown in Fig. 3, the model is able to capture the increase in the resonance frequency when the medium is changed from air to He. This effect is also visible in the experimental data.

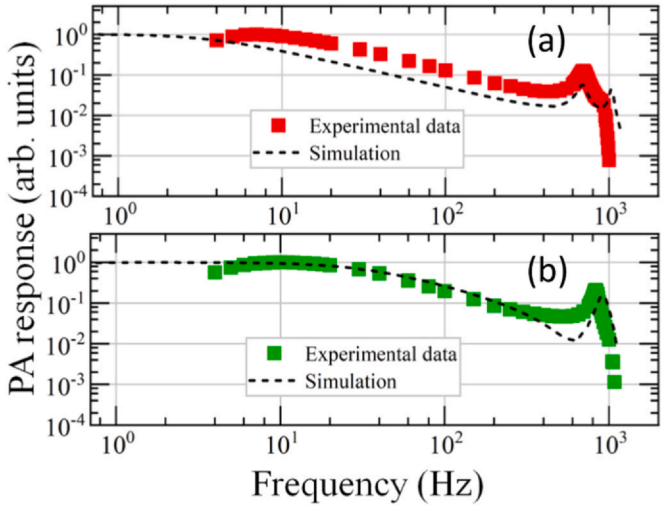

Fig. 3. Frequency response study of cantilever-I for (a) air and (b) He. The experimental data represent the PA response at different chopping frequencies. The dotted line depicts the result of numerical simulation which shows the amplitude of the cantilever displacement for different values of the modulating frequency.

To analyze the effect of the cantilever dimensions on the sensitivity of the PA detector, three additional cantilever geometries were studied by using the numerical model. Table 3 contains the dimensions, responses, and corresponding resonance frequencies of the cantilevers. Cantilever-II has the same length and width, but the thickness is twice that of cantilever-I. Hence, the effect of thickness can be checked from the obtained results in Fig. 4(a) and (b) and in Table 3, where the deflection amplitude is less compared to cantilever-I for air and He, respectively, at 40 Hz chopping frequency. To check the effect of length, the results of cantilever-III and cantilever-II can be compared. Both cantilevers have the same width and thickness, but the length of cantilever-III is shorter compared to cantilever-II and the result depicts more deflection amplitude for the longer cantilever. Cantilever-III has the same length and thickness as cantilever-IV, but the width is less resulting in increased deflection amplitude compared to cantilever-IV.

The frequency responses of the cantilevers in air and He are shown in Fig. 4(c)-(f). The resonance frequency is comparatively higher for cantilevers of shorter length, but all cantilevers have considerably high resonance frequencies compared to the operational frequency, which in our case, typically stays within 30–50 Hz. The cantilever dimensions can be tailored to improve the sensitivity (deflection amplitude) according to the obtained results of the model, by designing the cantilever longer and thinner with smaller width. However, there are technological limitations which prohibit the flexibility in choosing the dimensions, as a long and thin cantilever can introduce additional signal noise and the possibility of mechanical damage under comparatively higher gaseous pressure increases. The cantilever width could be made smaller to improve the PA signal strength but, in the simulations presented here width limit was kept at 0.7 mm for maintaining compatibility with the beam size of the displacement-sensing interferometer. Hence, the experiments were carried out using the cantilever-I design which gave the highest sensitivity. The following sections contain the results on the performance of the PA power detector using the cantilever-I.

4. Results and discussions

The evolution of PA signal S_{PA} with the increments of the incident radiation power at 1523 nm wavelength for gaseous medium air and

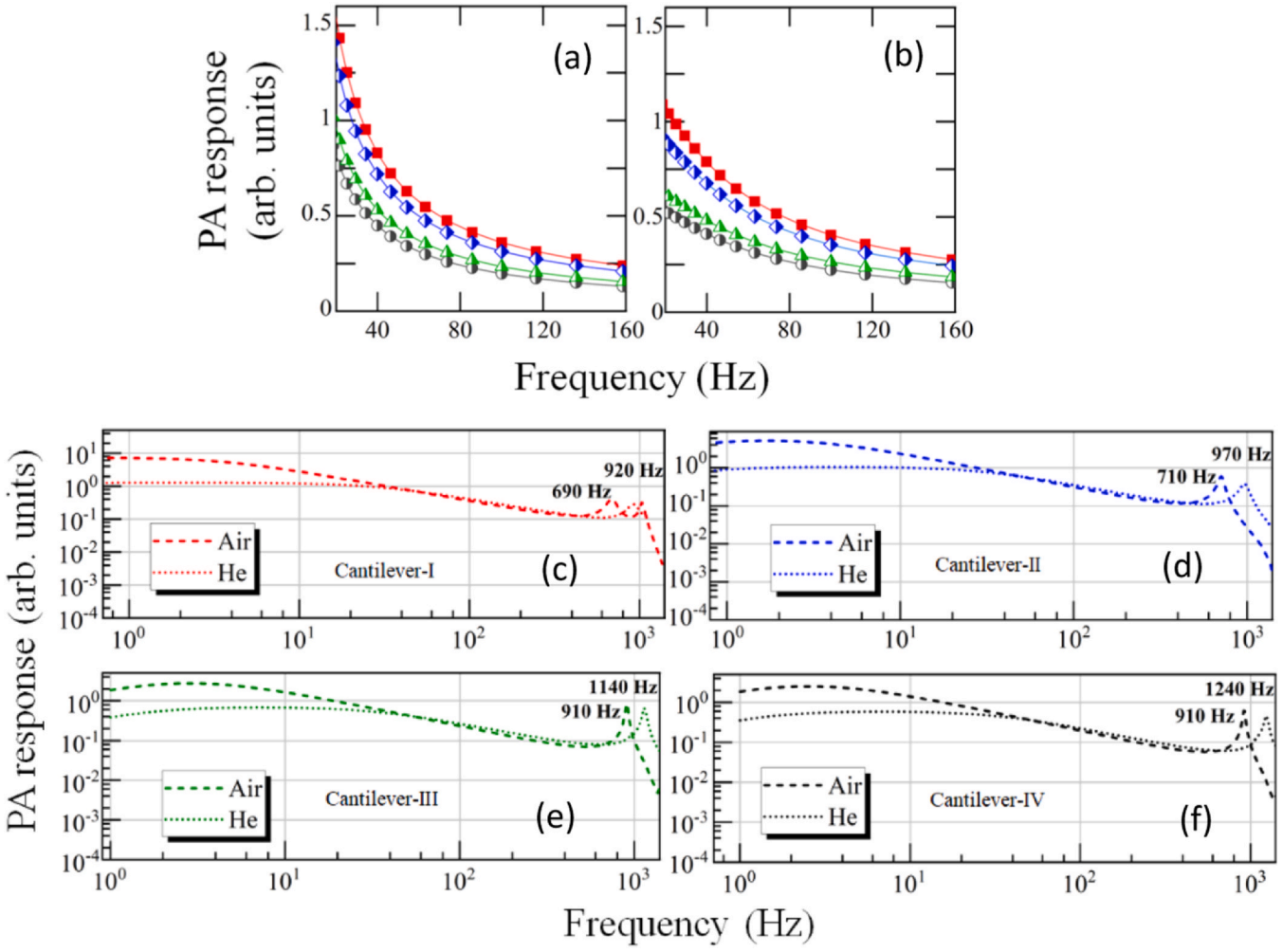

Fig. 4. Results of the numerical simulation for (a) air and (b) He on the change of signal strength in the frequency region from 20 Hz to 160 Hz for cantilever-I (red filled square) compared to cantilever-II (blue half-filled square), cantilever- III (green half-filled triangle) and cantilever-IV (black half-filled circle). (c)-(f) Frequency response of cantilever-I, II, III and IV. The resonance frequency becomes higher when the system is operated with He as the gaseous medium as compared to air.(For interpretation of the references to colour in this figure, the reader is referred to the web version of this article.)

He, is shown in Fig. 5(a)-(b). The grey area in the graph represents the background noise which limits the lowest detectable power.

Fig. 6(a)-(h) show linearity of the PA peak amplitude with respect to the incident power. The experimental data indicate the lowest detectable power of about 15 nW. Another important feature of this detection process is the large dynamic range. Fig. 5(b), (c), (f) and (g) show that the detection technique can be applied from 15 nW to 6 mW to achieve a dynamic range of nearly six orders of magnitude in both air and He. The wavelength dependence of the PA detection sensitivity σ_{PA} in air and He is shown in Fig. 7(a) and (b) at 325 nm, 442 nm, 633 nm and 1523 nm incident radiation wavelengths. The arbitrary units of the PA signal are the same for all figures.

Table 4 summarizes the sources of uncertainty components for the measurement. Apart from the uncertainty due to reproducibility of the results and linear fitting, the estimated sensitivities of Fig. 7 have measurement uncertainties due to the reference detector calibration, spatial nonuniformity of the PA responsivity and spectral transmittance of the window. Reproducibility was tested by repeating the measurement in another laboratory room. Relative uncertainties due to linear fitting were obtained from the data in Fig. 6. Silicon photodiode detector traceable to a pyroelectric detector has measurement uncertainty of 0.6% in the reference power measurement for 325 nm [30]. For 442 nm and 633 nm wavelengths, the reference power was measured using the same Silicon photodiode detector which is traceable to a predictable quantum efficient detector [31] with standard uncertainty of 0.25%. Indium gallium arsenide (InGaAs) detector traceable to the pyroelectric detector has standard uncertainty of 1.15% for 1523 nm [32].

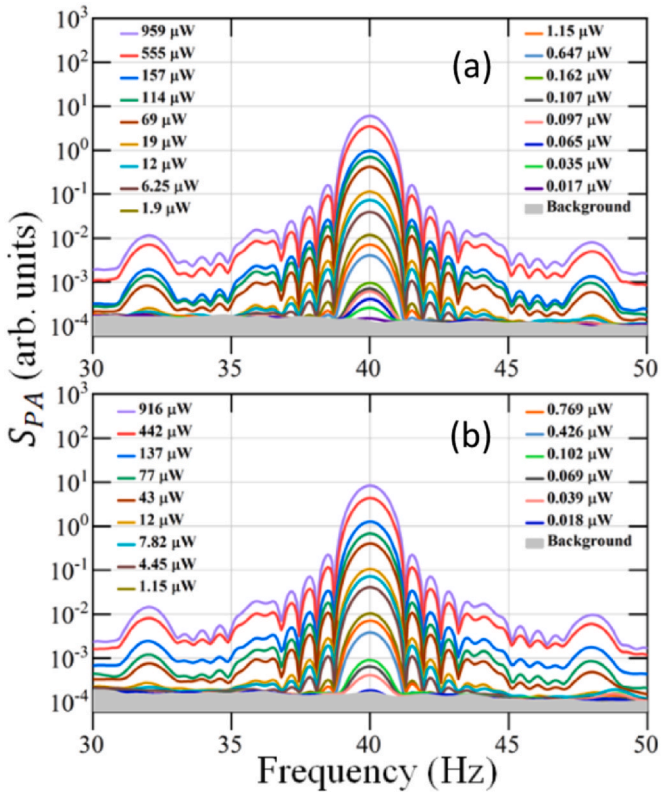

Fig. 5. PA peak amplitude increment with the increase of incident radiation intensity for gaseous medium (a) air and (b) He. The grey region represents the background noise signal.

The nonuniform spatial responsivity as indicated in Fig. 2 causes uncertainty in the PA sensitivity estimation because of the different beam diameters of the employed wavelengths. The $1/e^2$ beam diameter varied between 0.8 mm and 1.0 mm for other wavelengths than 442 nm where the beam diameter was 1.4 mm. In order to calculate the correction factor due to the larger beam size for 442 nm, the data of the responsivities measured at different spatial points with 0.5 mm scanning interval were employed. Two concentric Gaussian-like beam profiles of the same total power with diameters of 0.8 mm and 1.4 mm were placed at the measurement position. The corresponding responses were calculated based on Fig. 2 with additional responsivity values interpolated between the measured responsivities. The calculated response for the 0.8 mm beam profile was larger than that for the 1.4 mm beam profile by a factor of 1.027. Using reasonable variation of the related parameters, the correction factor was estimated to have a standard uncertainty of 0.009. Hence, a correction factor of 1.027 ± 0.009 was determined for the value of σ_{PA} measured at the wavelength of 442 nm to be compatible with the data at other wavelengths. The effect of variations in beam diameter at 325 nm, 633 nm and 1523 nm is covered by the uncertainty of 0.5% related to the measurement reproducibility.

Spectral transmittance of the Potassium Bromide (KBr) window plays an important role in the estimation of the detection sensitivity. The transmittance at 1523 nm was taken as the reference with respect to which the transmittance at shorter wavelengths was corrected. Hence, corrections due to the window transmittance by 1.068, 1.039 and 1.019 with a standard uncertainty of 0.003 were applied to the sensitivities at the wavelengths of 325 nm, 442 nm and 633 nm, respectively, relative to the sensitivity at 1523 nm. Adding quadratically the different uncertainty components of σ_{PA} yields the combined relative standard uncertainties given in Table 4.

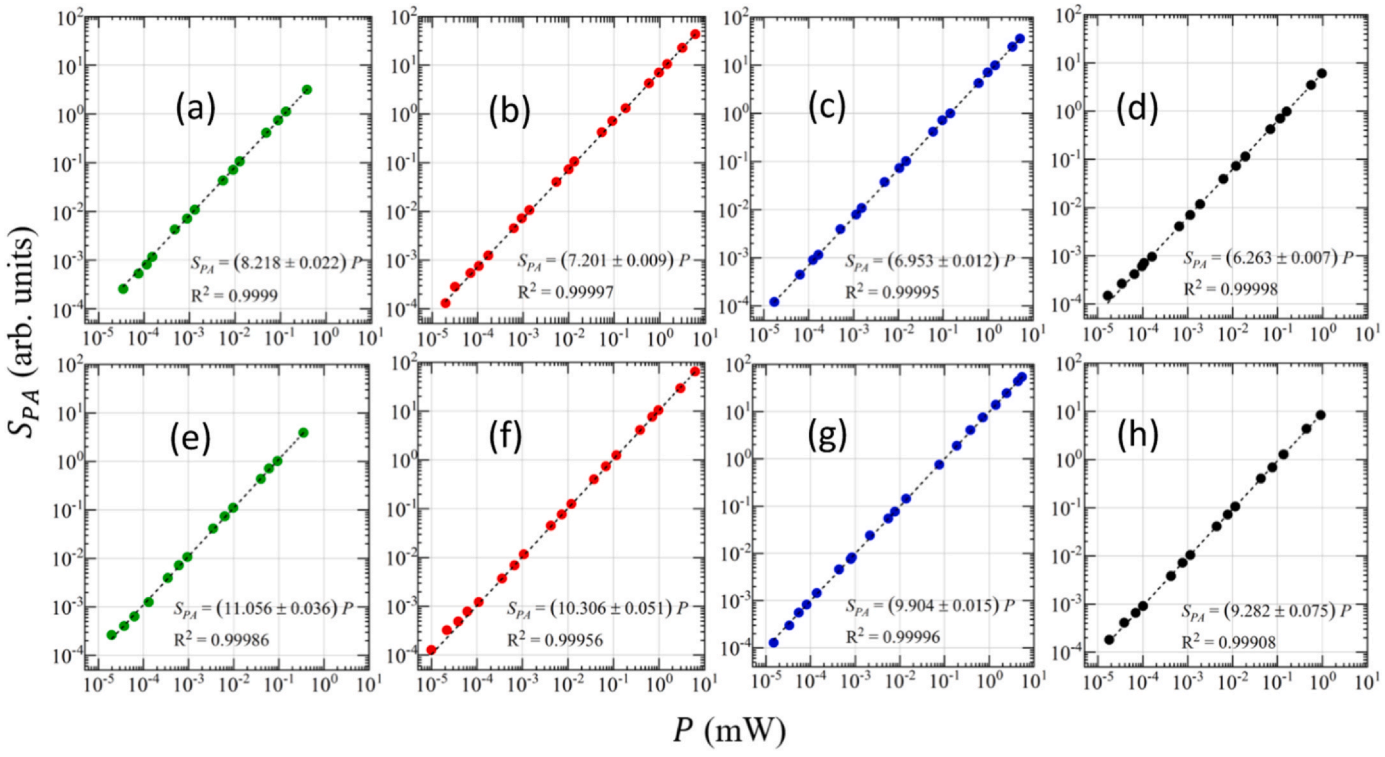

Fig. 6. Generated PA response with incident radiation power from ~ 15 nW to ~ 6 mW at 40 Hz chopping frequency under gaseous medium air (row 1: (a) - (d)) and He (row 2: (e) - (h)). The excitation wavelengths are: 325 nm (column 1), 442 nm (column 2), 633 nm (column 3) and 1523 nm (column 4). The dashed lines represent the linear fit (all linear regressions are passing through the origin). The values of R^2 for all the datasets are close to 1 suggesting good linearity. The PA signal amplitude (S_{PA}) has higher detection sensitivity (σ_{PA}) for He compared to air for the wavelengths between 325 nm and 1523 nm.

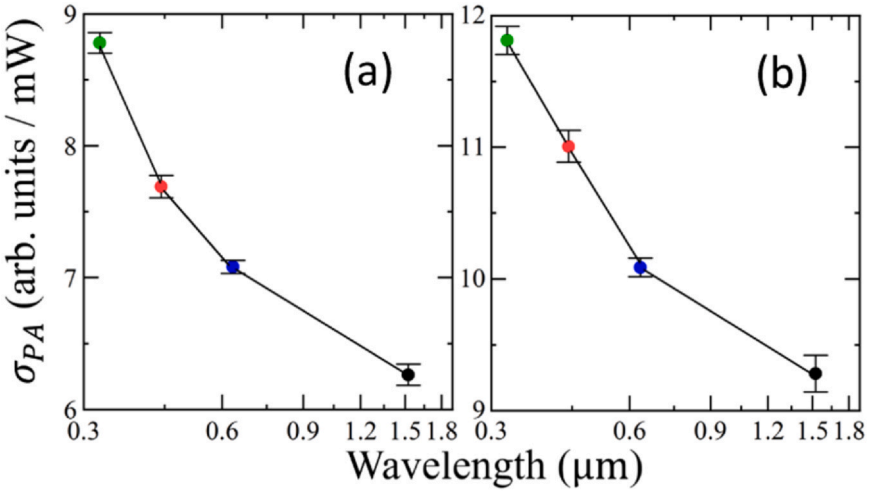

Fig. 7. Detection sensitivities, σ_{PA}, at different wavelengths of incident radiation. The value of the estimated σ_{PA} decreases by 21–29% as the wavelength increases for both (a) air and (b) He, respectively. The uncertainty bars indicate the combined standard uncertainty.

Table 4
Sources of uncertainty in the measurement of σ_{PA}.

Sources of uncertainty	Relative standard uncertainty (%)							
	Air				He			
	325 nm	442 nm	633 nm	1523 nm	325 nm	442 nm	633 nm	1523 nm
Reproducibility	0.50	0.50	0.50	0.50	0.50	0.50	0.50	0.50
Linear fitting	0.27	0.13	0.17	0.11	0.33	0.49	0.15	0.81
Reference power measurement	0.60	0.25	0.25	1.15	0.60	0.25	0.25	1.15
Spatial nonuniformity	-	0.90	-	-	-	0.90	-	-
Window transmittance	0.30	0.30	0.30	0.30	0.30	0.30	0.30	0.30
Combined standard uncertainty	0.9	1.1	0.7	1.3	0.9	1.2	0.7	1.5

5. Conclusions

In conclusion, we have implemented a cantilever-based PA radiation detection system, which is capable of detecting radiation power level ranging from 15 nW to ~ 6 mW, indicating a linear dynamic range of nearly six orders of magnitude. We have developed a numerical model that can be employed to optimize the PA detector design for radiation power measurements. Four different cantilever dimensions have been studied through simulations. Cantilever-I which showed better signal strength compared to other cantilevers, has been employed for the experiments. The experimentally measured and simulated resonance frequency of the system agree within 10%. We have verified that the power detection scheme can be employed for the spectral region ranging from 325 nm to 1523 nm. To check the linearity and the detection sensitivity, we have performed experiments with four laser wavelengths 325 nm, 442 nm, 633 nm, and 1523 nm. The result shows good linearity for both air and He gaseous media inside the PA cell. In the future, the detection ability will be tested up to THz range after employing a suitable window material in the setup. However, the present work verifies the potential of the cantilever-based PA detection system which can replace the need of multiple detection schemes for measuring electromagnetic radiation power in the nW to mW range with spectral range coverage from UV to NIR.

Author statement

MV and EI: Planned the research work and provided comments on various drafts of the manuscript, **JR and JU:** Provided the target sample, helped in troubleshooting of the photoacoustic detector operation, and also provided comments on the manuscript, **TL and FM:** Provided guidance for carrying out the experiments and helped in using different measuring instruments, and provided comments on the manuscript, **SS:** Developed the numerical model, performed the experiments, analyzed the results, wrote the first draft of the manuscript, and made revisions according to the suggestions of co-authors and referees.

Declaration of Competing Interest

The authors declare that they have no known competing financial interests or personal relationships that could have appeared to influence the work reported in this paper.

Acknowledgments

This project is funded by the Academy of Finland Flagship Programme, Photonics Research and Innovation (PREIN), Finland, decision number: 320167. The project is also a part of Universal Electromagnetic Radiation Detector (UNIDET) research project, which is funded by the Academy of Finland, Finland, (Project numbers 314363 and 314364). We thank Janne Askola for helping with the experiments on the spatial scan.

References

[1] S. Manohar, D. Razansky, Photoacoustics: a historical review, Adv. Opt. Photon. 8 (2016) 586.
[2] F. Gao, R. Kishor, X. Feng, S. Liu, R. Ding, R. Zhang, Y. Zheng, An analytical study of photoacoustic and thermoacoustic generation efficiency towards contrast agent and film design optimization, Photoacoustics 7 (2017) 1–11.

[3] W.-Y. Chang, X. Zhang, J. Kim, W. Huang, A. Bagal, C. Chang, T. Fang, H. Wu, X. Jiang, Evaluation of photoacoustic transduction efficiency of candle soot nanocomposite transmitters, IEEE Trans. Nanotechnol. 17 (2018) 985–993.
[4] J. Kim, H. Kim, W. Chang, W. Huang, X. Jiang, P. Dayton, Candle-soot carbon nanoparticles in photoacoustics: advantages and challenges for laser ultrasound transmitters, IEEE Nanotechnol. Mag. 13 (2019) 13–28.
[5] K. Chamassi, W. Trzpil, R. Arinero, R. Rousseau, A. Vicet, M. Bahriz, Capacitive silicon micro-electromechanical resonator for enhanced photoacoustic spectroscopy, Appl. Phys. Lett. 115 (2019) 081106.
[6] T. Tomberg, T. Hieta, M. Vainio, L. Halonen, Cavity-enhanced cantilever-enhanced photoacoustic spectroscopy, Analyst 144 (2019) 2291–2296.
[7] K. Chen, B. Zhang, S. Liu, Q. Yu, Parts-per-billion-level detection of hydrogen sulfide based on near-infrared all-optical photoacoustic spectroscopy, Sens. Actuators B Chem. 283 (2019) 1–5.
[8] C. Wynn, S. Palmacci, M. Clark, R. Kunz, Dynamic photoacoustic spectroscopy for trace gas detection, Appl. Phys. Lett. 101 (2012) 184103.
[9] Wei Li, Zihu Wang, Chuhuan Feng, Qi Li, Hongbin Yu, High sensitivity all-optical acoustic pressure sensor based on resonantmicro-opto-mechanical cantilever with integrated rib waveguide, Sens. Actuators A 285 (2019) 300–307.
[10] Y. He, Y. Ma, Y. Tong, X. Yu, F.K. Tittel, A portable gas sensor for sensitive CO detection based on quartz-enhanced photoacoustic spectroscopy, Opt. Laser Technol. 115 (2019) 129–133.
[11] L. Wang, C. Zhang, L. Wang, Grueneisen relaxation photoacoustic microscopy, Phys. Rev. Lett. 113 (2014) 174301.
[12] A.C. Tam, Applications of photoacoustic sensing techniques, Rev. Mod. Phys. 58 (1986) 381–431.
[13] L. Wang, S. Hu, Photoacoustic tomography: in vivo imaging from organelles to organs, Science 335 (2012) 1458-62.
[14] J. Peltola, T. Hieta, M. Vainio, Parts-per-trillion-level detection of nitrogen dioxide by cantilever-enhanced photo-acoustic spectroscopy, Opt. Lett. 40 (2015) 2933.
[15] I. Kauppinen, A. Branders, J. Uotila, J. Kauppinen and T. Kuusela, Sensitive and fast gas sensor for wide variety of applications based on novel differential infrared photoacoustic principle, SENSOR+TEST Conferences 2011, 71–75.
[16] K. Wilcken, J. Kauppinen, Optimization of a microphone for photoacoustic spectroscopy, Appl. Spectrosc. 57 (2003) 1087-92.
[17] T. Laurila, H. Cattaneo, T. Pöyhönen, V. Koskinen, J. Kauppinen, R. Hernberg, Cantilever-based photoacoustic detection of carbon dioxide using a fiber-amplified diode laser, Appl. Phys. B 83 (2006) 285–288.
[18] C.L. Tan, H. Mohseni, Emerging technologies for high performance infrared detectors, Nanophotonics 7 (2018) 169–346.
[19] T.R. Gentile, J.M. Houston, G. Eppeldauer, A.L. Migdall, C.L. Cromer, Calibration of a pyroelectric detector at 10.6 mm with the National Institute of Standards and Technology high-accuracy cryogenic radiometer, Appl. Opt. 36 (1997) 3614–3618.
[20] J.W. Stewart, J.H. Vella, W. Li, S. Fan, M.H. Mikkelsen, Ultrafast pyroelectric photodetection with on-chip spectral filters, Nat. Mater. 19 (2020) 158–162.
[21] V.E. Rogalina, I.A. Kaplunov, G.I. Kropotovc, Optical materials for the THz range, Opt. Spectrosc. 125 (2018) 1053–1064.
[22] Y. Li, Z. Guo, G. Li, S. Chen, Miniature fiber-optic high-intensity focused ultrasound device using a candle soot nanoparticles-polydimethylsiloxane composites-coated photoacoustic lens, Opt. Express 26 (2018) 21700–21711.
[23] J. Lehman, C. Yung, N. Tomlin, D. Conklin, M. Stephens, Carbon nanotube-based black coatings, Appl. Phys. Rev. 5 (2018) 011103.
[24] R. Willems, P. Bakker, N. Dam, Laser-induced incandescence versus photo-acoustics: implications for qualitative soot size diagnostics, Appl. Phys. B 125 (2019) 138.
[25] J. Lehman, A. Steiger, N. Tomlin, M. White, M. Kehrt, I. Ryger, M. Stephens, C. Monte, I. Mueller, J. Hollandt, M. Dowell, Planar hyperblack absolute radiometer, Opt. Express 24 (2016) 25911–25921.
[26] J. Rossi, J. Uotila, S. Sharma, T. Laurila, R. Teissier, A. Baranov, E. Ikonen, M. Vainio, Photoacoustic characteristics of carbon-based infrared absorbers, Photoacoustics 23 (2021) 100265.
[27] COMSOL Multiphysics® Acoustics Module User's Guide. Version 5.4.
[28] A. Maali, C. Hurth, R. Boisgard, C. Jai, T. Cohen-Bouhacina, J. Aimé, Hydrodynamics of oscillating atomic force microscopy cantilevers in viscous fluids, J. Appl. Phys. 97 (2005) 074907.
[29] G.P. Ward, R.K. Lovelock, A.R.J. Murray, A.P. Hibbins, J.R. Sambles, Boundary-layer effects on acoustic transmission through narrow slit cavities, Phys. Rev. Lett. 115 (2015) 044302.
[30] L. Werner, Final report on the key comparison CCPR-K2.c-2003: spectral responsivity in the range of 200 nm to 400 nm, Metrologia 51 (2014) 02002.
[31] T. Donsberg, M. Sildoja, F. Manoocheri, M. Merimaa, L. Petroff, E. Ikonen, A primary standard of optical power based on induced-junction silicon photodiodes operated at room temperature, Metrologia 51 (2014) 197–202.
[32] K. Maham, A. Vaskuri, F. Manoocheri, E. Ikonen, Calibration of near-infrared detectors using a wavelength tunable light source, Opt. Rev. 27 (2020) 183–189.

Sucheta Sharma received the M.Sc. degree in Physics from the University of Calcutta, India, in 2014. She is currently a Doctoral candidate at Aalto University, Finland.

Toni Laurila is a Research Fellow at Aalto University, Finland, and the CEO of Sensmet Oy.

Jussi Rossi is currently a Doctoral Researcher at Tampere University, Finland.

Juho Uotila is a Senior System Specialist at Patria Aviation Oy. He received the M.Sc. and Ph.D. degrees in Physics from University of Turku, Finland, in 2003 and 2009 respectively.

Markku Vainio is an Associate Professor at the department of Chemistry of University of Helsinki, Finland and a Senior Researcher at the Photonics Laboratory of Tampere University, Finland.

Farshid Manoocheri is currently a Staff Scientist of Metrology Research Institute, at the department of Signal Processing and Acoustics of Aalto University, Finland.

Erkki Ikonen is a Professor of Measurement Science and Technology at the department of Signal Processing and Acoustics of Aalto University and Research Professor at VTT Technical Research Centre of Finland. He received the M.Sc. and D.Sc. (Tech.) degrees in engineering from the Helsinki University of Technology, Espoo, Finland, in 1982 and 1988, respectively.